Trench Waves[1]

LAWRENCE A. MYSAK,[2] PAUL H. LEBLOND AND WILLIAM J. EMERY

Institute of Oceanography, University of British Columbia, Vancouver, B.C., Canada, V6T 1W5

(Manuscript received 4 September 1978, in final form 26 March 1979)

ABSTRACT

The cross sections of four trenches peripheral to the Pacific Ocean are fitted by a double exponential depth profile. Nondivergent trapped wave propagation is shown to be possible in two directions along such a profile. In addition to the familiar shelf waves, only slightly modified by the presence of a trench, "trench waves" propagating in the direction opposite to that of shelf waves and at speeds lower by an order of magnitude are also possible.

Dispersion curves and eigenfunctions are presented for the Peru-Chile and Japan-Kuril trenches. Coastal sea level records are used to demonstrate phase propagation at "trench wave" phase speeds off both Japan and Peru. The fundamental mode speeds predominate in the phase spectra off both Japan and Peru.

1. Introduction

The role played by the continental shelf in guiding long-wave energy along oceanic boundaries is now well understood. The properties of coastal trapped long waves traveling along various monotonic depth profiles that model the continental shelf/slope region have been recently reviewed by LeBlond and Mysak (1977, 1978), and the general qualitative theory of these waves has been discussed by Huthnance (1975, 1978). In particular, we recall here that in the absence of strong longshore currents, second-class shelf waves always propagate their phase with the shallow water (i.e., the coast) to the right (left) in the Northern (Southern) Hemisphere. Further, the amplitude of a shelf wave decays rapidly away from the edge of the shelf. Shelf waves with periods of several days were first observed on the east Australian coast by Hamon (1962, 1963), and their presence has since been detected along many coastlines (see above reviews).

In some coastal areas, the depth of the ocean does *not* increase monotonically away from the shoreline because of the presence of banks or trenches. The reversal in bottom slope associated with such a feature raises the possibility of another set of second-class waves coexisting with the shelf waves, but propagating their phase in the opposite direction to the latter. Also, the energy of this set of waves is likely to be trapped over the bank or trench. Second-class wave propagation along a coast with a bank offshore, on the shelf, has recently been investigated by Louis (1978). As a model of the Hecate Bank off the coast of Oregon, Louis used the following form for the depth profile $H(x)$:

$$H(x) = \begin{cases} H_1, & -L_1 \leq x < 0 \\ H_2, & 0 < x < L_2 \\ H_3, & L_2 < x < \infty \end{cases} \qquad (1.1)$$

where x denotes the distance normal to the coast and the H_i are constants, with $H_2 < H_1 \leq H_3$. In agreement with the above remarks regarding phase propagation, Louis indeed found that second-class waves travel in both directions along the above depth profile.

We observe that (1.1) can also be used as a crude model for a coastal trench if we specify that $H_1 \leq H_3 < H_2$. An examination of a number of such trenches in the Pacific Ocean reveals, however, that their form is much more accurately represented by a pair of exponential depth profiles with slopes of opposite sign. It is the propagation of barotropic second-class waves along this type of bathymetry which we shall discuss in this paper. Along a coast bordered by such a trench, typically the kind of bathymetry found in subduction zones at plate boundaries, one expects two types of second-class waves: 1) continental shelf waves, which propagate their phase according to the criterion given in the first paragraph, and 2) trench waves, which propagate their phase in the direction opposite to that of the shelf waves. Further, one anticipates that the energy of shelf and trench waves will be

[1] Dedicated to Professor George L. Pickard on the occasion of his retirement.

[2] Also Department of Mathematics, University of British Columbia.

0022-3670/79/051001-13$07.25

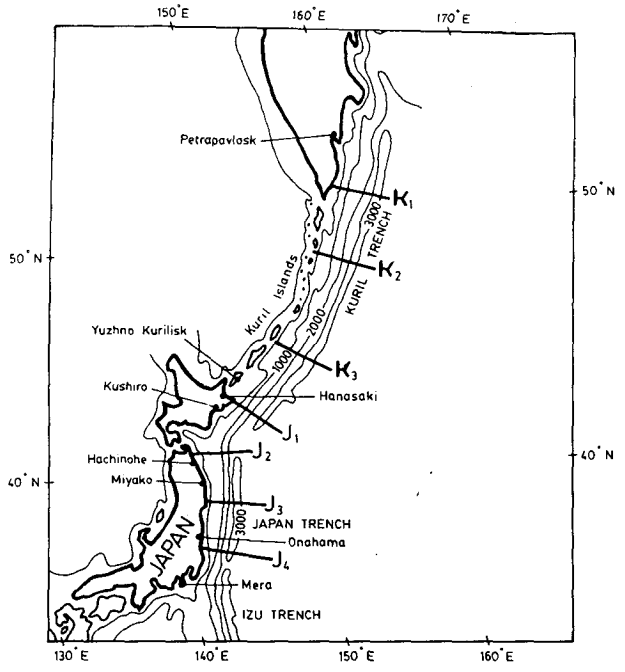

FIG. 1. Map of the Japan and Kuril trenches and the sea level stations used in the analysis. Sections labeled J and K are those along which depth profiles were taken. Depth contours are in fathoms.

trapped over the shelf and trench regions respectively.

Recently, by using current meter data from moorings off Peru, Smith (1978) was able to confirm poleward phase propagation at speeds slightly greater than that expected for shelf waves. Similar evidence of poleward propagation was found using lag-correlations and cross-spectral comparisons of coastal sea level data. These techniques, applied to somewhat longer records of daily sea level from Peru, also indicate equatorward propagation at the nondispersive phase speed of the fundamental mode trench wave. Using monthly sea level data from many stations along the Japan-Kuril trench system, these techniques confirm northward propagation, consistent with trench wave dynamics, at speeds representative of the first three trench wave modes.

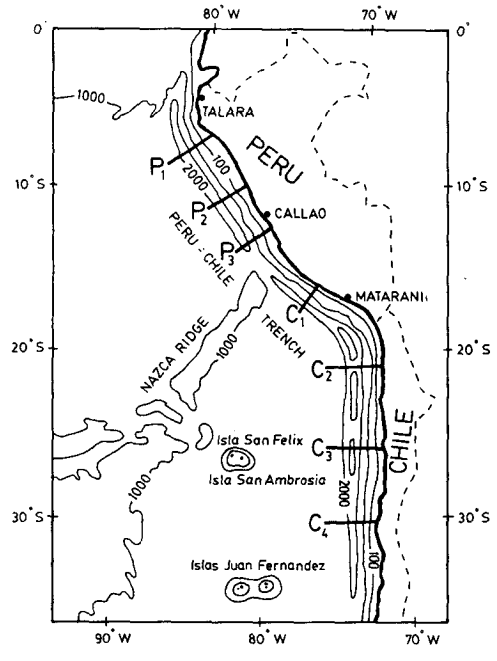

FIG. 2. Map of the Peru-Chile trench and coastal sea level stations employed. Sections labeled P and C are those along which depth profiles were taken. Depth contours are in fathoms.

2. Trench profiles

We have chosen to examine two trench systems on the periphery of the Pacific Ocean: the Japan-Kuril and Peru-Chile trenches. The locations of these trenches and of the bathymetric transects used to determine their depth profiles are shown in Figs. 1 and 2. As a simple approximation to the depth profiles shown in Fig. 3, we have used a depth function of the form

$$H(x) = \begin{cases} H_1 = H_0 e^{2\alpha x}, & -L_1 \leq x \leq 0 \\ H_2 = H_0 e^{-2\beta x}, & 0 \leq x \leq L_2 \\ H_3 = H_0 e^{-2\beta L_2}, & L_2 \leq x \leq \infty. \end{cases} \quad (2.1)$$

The origin ($x = 0$) is taken at the deepest point of the trench. The fitted profile for each trench is also shown in Fig. 3; the values of the parameters α, β, L_1, L_2, H_0 are listed in Table 1.

It is convenient to introduce the nondimensional parameters

$$a = \alpha L_1, \quad b = \beta L_1, \quad r = L_2/L_1, \quad (2.2)$$

which will be used later in the mathematical analysis. The depth profile (2.1) then takes the form

$$H(x') = \begin{cases} H_0 e^{2ax'}, & -1 \leq x' \leq 0 \\ H_0 e^{-2bx'}, & 0 \leq x' \leq r \\ H_0 e^{-2br}, & 0 \leq x' < \infty \end{cases} \quad (2.3)$$

with $x' = x/L_1$. The values of a, b and r for the various trenches are also given in Table 1.

3. Governing equations

The unforced linearized equations for barotropic, nondivergent motions on an f-plane with depth profile $H(x)$ are given by

$$u_t - fv + \rho^{-1}p_x = 0, \quad (3.1a)$$

$$v_t + fu + \rho^{-1}p_y = 0, \quad (3.1b)$$

$$(Hu)_x + Hv_y = 0, \quad (3.2)$$

where u, v are the velocity components in the x, y directions, p is the pressure, ρ the density and f the constant Coriolis parameter. The coordinates x, y, z form a right-handed system with x directed away from the coast (at $x = -L_1$), y along the

coast and z upward. In view of the nondivergent form of (3.2) (i.e., the rigid-lid approximation, which filters out all gravity waves in the system), the velocity components can be expressed in terms of a mass transport streamfunction $\Psi(x,y,t)$:

$$u = -\Psi_y/H, \quad v = \Psi_x/H. \tag{3.3}$$

Substituting (3.3) into (3.1a,b), eliminating p, and then taking Ψ to have the plane wave form

$$\Psi = \psi(x)e^{i(ky-\omega t)}, \quad k > 0, \tag{3.4}$$

we obtain the vorticity balance equation (cf. LeBlond and Mysak, 1978, p. 237)

$$\left(\frac{\psi'}{H}\right)' + \left[\frac{fk}{\omega}\left(\frac{1}{H}\right)' - \frac{k^2}{H}\right]\psi = 0, \tag{3.5}$$

where the prime denotes differentiation with respect to x.

We shall assume that (3.5) holds in the interval $-L_1 \leq x < \infty$; at the end points we impose the boundary conditions

$$\psi = 0 \quad \text{at} \quad x = -L_1, \tag{3.6}$$

$$\psi \to 0 \quad \text{as} \quad x \to \infty, \tag{3.7}$$

which imply that there is no transport across the shoreline at $x = -L_1$ and that the waves are trapped against the coast. At a discontinuity in H or H', at x_0 say, we require that the normal transport Hu and the pressure p be continuous. These imply the jump conditions

$$[\psi] = 0 \quad \text{at} \quad x = x_0, \tag{3.8}$$

$$\left[\frac{\psi' + (fk/\omega)\psi}{H}\right] = 0 \quad \text{at} \quad x = x_0. \tag{3.9}$$

For the steplike profile (1.1), these conditions must be applied at $x = 0$ and $x = L_2$. For the double exponential profile (2.1), in which H is continuous, (3.8) must be applied at $x = 0$ and $x = L_2$ and (3.9) reduces to

$$[\psi'] = 0 \quad \text{at} \quad x = 0, L_2. \tag{3.10}$$

4. Derivation of general dispersion relation

In the shelf region $-L_1 \leq x \leq 0$, Eq. (3.5) with depth profile $H_1(x)$ given by (2.1) reduces to

$$\psi_1'' - 2\alpha\psi_1' - (2fk\alpha/\omega + k^2)\psi_1 = 0, \quad -L_1 \leq x \leq 0. \tag{4.1}$$

The equation for ψ_2 in the trench region $0 \leq x \leq L_2$ is obtained from (4.1) by replacing α by $-\beta$. In the deep-sea region $L_2 \leq x < \infty$, Eq. (3.5) simply becomes

$$\psi_3'' - k^2\psi_3 = 0, \quad L_2 \leq x < \infty. \tag{4.2}$$

The function ψ which satisfies the above equations, the boundary conditions (3.6), (3.7), and the jump

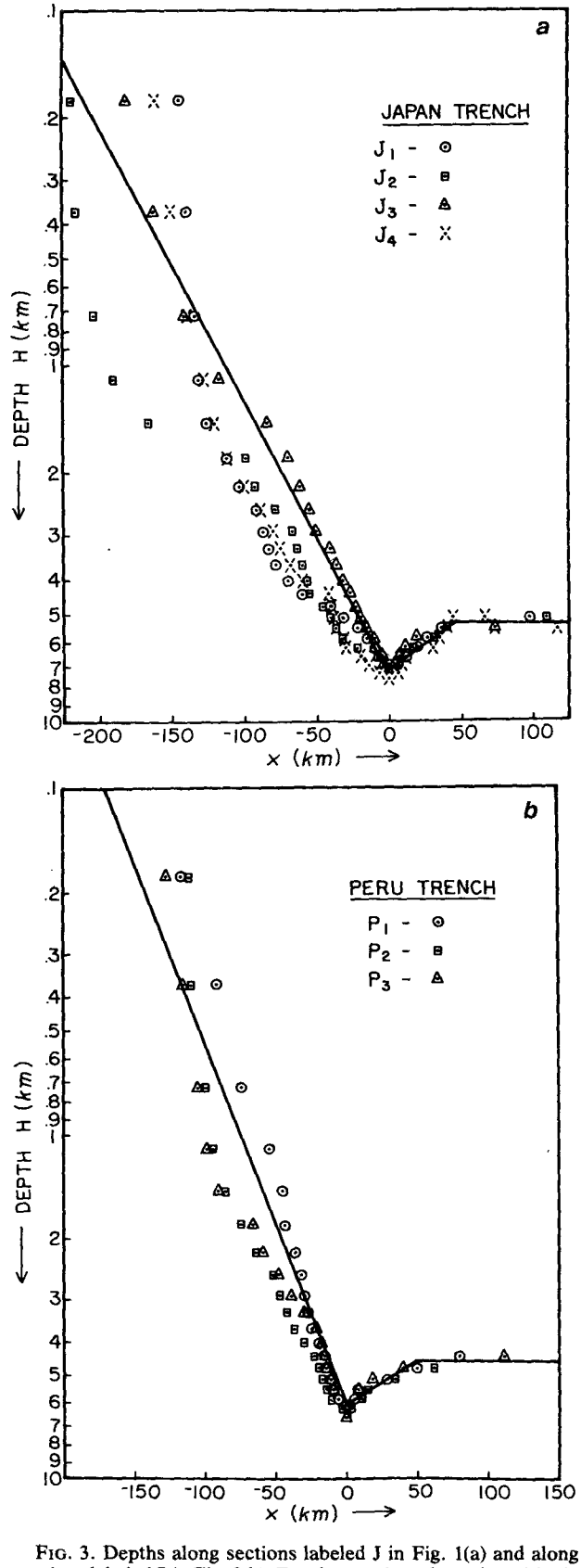

FIG. 3. Depths along sections labeled J in Fig. 1(a) and along sections labeled P in Fig. 2(b). Depths are plotted on a logarithmic scale with actual depths as points and the fitted curve as a solid line.

condition (3.8) at $x = 0$, L_2 is given by

$$\psi = \begin{cases} \psi_1 = Ae^{\alpha x} \sin m(x + L_1), & -L_1 \leq x \leq 0 \\ \psi_2 = e^{-\beta x}(B \sin lx + A \sin mL_1 \cos lx), & 0 \leq x \leq L_2 \\ \psi_3 = e^{-\beta L_2}(B \sin L_2 + A \sin mL_1 \cos lL_2)e^{-k(x-L_2)}, & L_2 \leq x \leq \infty, \end{cases} \quad (4.3)$$

where

$$m = (-2\alpha fk/\omega - \alpha^2 - k^2)^{1/2}, \quad (4.4a)$$

$$l = (2\beta fk/\omega - \beta^2 - k^2)^{1/2}, \quad (4.4b)$$

and A and B are arbitrary constants.

The substitution of (4.3) into (3.10) yields two homogeneous equations for A and B. Upon setting the determinant of coefficients of these two equations equal to zero, we obtain the general dispersion relation

$$(\alpha + \beta + m \cot mL_1)[l + (k - \beta) \tan lL_2] + l(k - \beta - l \tan L_2) = 0. \quad (4.5)$$

In the limit $L_2 \to 0$ and $\beta \to 0$ (no trench), Eq. (4.5) reduces to

$$\tan mL_1 = -m/(k + \alpha), \quad (4.6)$$

in agreement with Buchwald and Adams (1968). In order for (4.6) to have an infinity of real positive roots m_n ($n = 0, 1, 2, \ldots$) for fixed k and α, the frequency must obey the inequality [see Eq. (4.4a)]

$$\frac{-2\alpha k}{\alpha^2 + \kappa^2} < \frac{\omega}{f} < 0. \quad (4.7)$$

Once the roots m_n of (4.6) are obtained, then (4.4a) is used to determine the shelf wave eigenfrequencies $\omega_n(k)$. The upper bound in (4.7) yields the shelf-wave phase propagation criterion referred to in the Introduction. Also, since (4.7) implies that $\omega/f \to 0$ as both $k \to 0$ and $k \to \infty$, it follows that each shelf wave mode has a zero group velocity at some intermediate value of k. We shall see below that this result regarding the group velocity also holds for trench waves.

Although of less practical importance, it nevertheless is of theoretical interest to note that in the limit $L_1 \to 0$ and $\alpha \to 0$ (no shelf), Eq. (4.5) yields

$$l + (k - \beta) \tan lL_2 = 0 \quad (4.8a)$$

or

$$\tan lL_2 = l/(k - \beta) \quad (4.8b)$$

provided $k \neq \beta$. If $k = \beta$, then (4.8a) implies that $l = 0$, in which case (4.4b) gives $\omega = f$; but this leads to the trivial solution $\psi_2 = 0 = \psi_3$ [cf. Eq. (4.3.)] In analogy with the shelf wave case, Eq. (4.8b) has real positive roots l_n provided that (see Eq. (4.4b)]

$$0 < \frac{\omega}{f} < \frac{2\beta k}{\beta^2 + k^2}. \quad (4.9)$$

Thus the direction of phase propagation for a pure trench wave is opposite to that of the shelf wave. We note, however, that (4.9) implies that the group velocity of each trench wave mode also vanishes at some intermediate value of k.

5. Dispersion relations and eigenfunctions for shelf waves and trench waves

As mentioned in the Introduction, the presence of both positive and negative bottom slopes in the shelf-trench profile (2.1) allows the existence of second-class waves traveling in opposite directions. To bring out this property more explicitly, we first define a nondimensional frequency and wavenumber

$$\sigma = \omega/f, \quad \kappa = kL_1 > 0. \quad (5.1)$$

In terms of these and the nondimensionalized geometric parameters a, b, r defined in Section 2, *viz.*,

$$a = \alpha L_1, \quad b = \beta L_1, \quad r = L_2/L_1, \quad (5.2)$$

the dispersion relation (4.5) takes the form

$$(a + b + \mu \cot \mu)[\lambda + (\kappa - b) \tan \lambda r] + \lambda(\kappa - b - \lambda \tan \lambda r) = 0, \quad (5.3)$$

where

$$\mu = (-2a\kappa/\sigma - a^2 - \kappa^2)^{1/2}, \quad (5.4a)$$

TABLE 1. Values of the parameters of fitted profiles of the form (2.1) to four trenches in the Pacific.

Trench	H_0 (km)	L_1 (km)	L_2 (km)	α (km^{-1})	β (km^{-1})	a ($=\alpha L_1$)	b ($=\beta L_1$)	r ($=L_2/L_1$)
Kuril	8.25	185	55	0.95×10^{-2}	4.24×10^{-3}	1.75	0.784	0.297
Japan	7.25	208	45	0.88×10^{-2}	3.27×10^{-3}	1.84	0.681	0.220
Japan-Kuril	7.75	197	50	0.91×10^{-2}	3.71×10^{-3}	1.80	0.730	0.260
Chile	6.24	107	50	1.32×10^{-2}	3.82×10^{-3}	1.41	0.409	0.467
Peru	6.06	171	50	1.20×10^{-2}	2.84×10^{-3}	2.04	0.486	0.292

$$\lambda = (2b\kappa/\sigma - b^2 - \kappa^2)^{1/2}. \quad (5.4b)$$

Eq. (5.3) represents an implicit form of the dispersion relation [$\sigma = \sigma(\kappa)$], with r, a and b as parameters. For fixed values of the latter, we wish to find the real solutions $\sigma_n(\kappa)$, $n = 0, 1, 2 \ldots$, of (5.3). For this purpose it is necessary to examine the cases of positive and negative σ separately.

When $\sigma < 0$ (shelf wave case), we see from (5.4b) that λ is pure imaginary. Thus for this case, we let $\lambda = iN$, where

$$N = (-2b\kappa/\sigma + b^2 + \kappa^2)^{1/2} > 0. \quad (5.5)$$

Under this transformation, Eq. (5.3) becomes

$$a + \kappa + \mu \cot\mu = \tanh Nr \times \left[\frac{b - \kappa}{N}(a + b + \mu \cot\mu) - N\right]. \quad (5.6)$$

In the limit $r \to 0$ (no trench), this reduces to

$$\tan\mu = -\mu/(\kappa + a), \quad (5.7)$$

which is the nondimensional form of (4.6). For (5.6) to have real roots $\sigma_n(\kappa)$, we require that [see (5.4a)].

$$\frac{-2a\kappa}{a^2 + \kappa^2} < \sigma < 0, \quad (5.8)$$

which is the nondimensional form of (4.7). Thus we conclude that even with a trench present, each shelf wave mode propagates in the expected direction and has a zero group velocity at some intermediate wavenumber. The largest negative root satisfying (5.6) and (5.8) will be denoted by σ_0 (the fundamental mode), the next largest negative root by σ_1 and so on:

$$\frac{-2a\kappa}{a^2 + \kappa^2} < \sigma_0 < \sigma_1 < \sigma_2 < \ldots < 0. \quad (5.9)$$

For a particular root $\sigma_n(\kappa)$, the corresponding nth mode shelf wave eigenfunction can be written as

$$\psi^{(n)} = \begin{cases} \psi_1^{(n)} = e^{ax'} \sin\mu(x' + 1), & -1 \leq x' \leq 0 \\ \psi_2^{(n)} = e^{-bx'}(B \sinh Nx' + \sin\mu \cosh Nx'), & 0 \leq x' \leq r \\ \psi_3^{(n)} = e^{-br}(B \sinh Nr + \sin\mu \cosh Nr)e^{-\kappa(x'-r)}, & r \leq x' < \infty \end{cases} \quad (5.10)$$

where

$$x' = x/L_1,$$

$$B = [(a + b) \sin\mu + \mu \cos\mu]/N \quad (5.11)$$

and $\mu = \mu(\sigma_n)$, $N = N(\sigma_n)$. Eq. (5.10) is the nondimensional form of (4.3) when $A = 1$ and $\sigma < 0$. The relation (5.11) is obtained upon requiring that ψ' be continuous at $x = 0$. Note that $\psi^{(n)}$ is oscillatory over the shelf region ($-1 \leq x' \leq 0$) and of exponential character over the trench and deep-sea regions.

When $\sigma > 0$ (trench wave case), μ is now pure imaginary and we thus put $\mu = iM$, where

$$M = (2a\kappa/\sigma + a^2 + \kappa^2)^{1/2} > 0. \quad (5.12)$$

Under this transformation, Eq. (5.3) becomes

$$\lambda + (\kappa - b) \tan\lambda r = \frac{\tanh M}{M}\{-\lambda(a + \kappa) + \tan\lambda r[\lambda^2 - (a + b)(\kappa - b)]\}. \quad (5.13)$$

The pure trench dispersion relation [cf. (4.8a)] can be formally obtained from (5.13) by setting the right side equal to zero. However, since $L_1 = 0$ ($r = \infty$) in this case, L_2 must now be used as the length scale. Thus the nondimensional form of (4.8a) can be written as

$$\lambda' + (\kappa' - b') \tan\lambda' = 0, \quad (5.14)$$

where

$$\kappa' = kL_2, \quad b' = \beta L_2,$$

$$\lambda' = (2b'\kappa'/\sigma - b'^2 - \kappa'^2)^{1/2}. \quad (5.15)$$

For (5.13) to have real roots $\sigma_n(\kappa)$, we require that [cf. (4.9)]

$$0 < \sigma < \frac{2b\kappa}{b^2 + \kappa^2}. \quad (5.16)$$

In analogy to the shelf wave case, the roots will be ordered as

$$0 < \ldots < \sigma_1 < \sigma_0 < \frac{2b\kappa}{b^2 + \kappa^2}. \quad (5.17)$$

For a particular root $\sigma_n(\kappa)$, the corresponding nth mode trench wave eigenfunction can be written as

$$\psi^{(n)} = \begin{cases} \psi_1^{(n)} = e^{ax'} \sinh M(x' + 1), & -1 \leq x' \leq 0 \\ \psi_2^{(n)} = e^{-bx'}(B \sin\lambda x' + \sinh M \cos\lambda x'), & 0 \leq x' \leq r \\ \psi_3^{(n)} = e^{-br}(B \sin\lambda r + \sinh M \cos\lambda r)e^{-\kappa(x'-r)}, & r \leq x' < \infty \end{cases} \quad (5.18)$$

where now

$$B = [(a + b) \sinh M + M \cosh M]/\lambda \quad (5.19)$$

and $\lambda = \lambda(\sigma_n)$, $M = M(\sigma_n)$. As expected, $\psi^{(n)}$ has an oscillatory behavior over the trench region ($0 \leq x' \leq r$) and is of exponential character elsewhere.

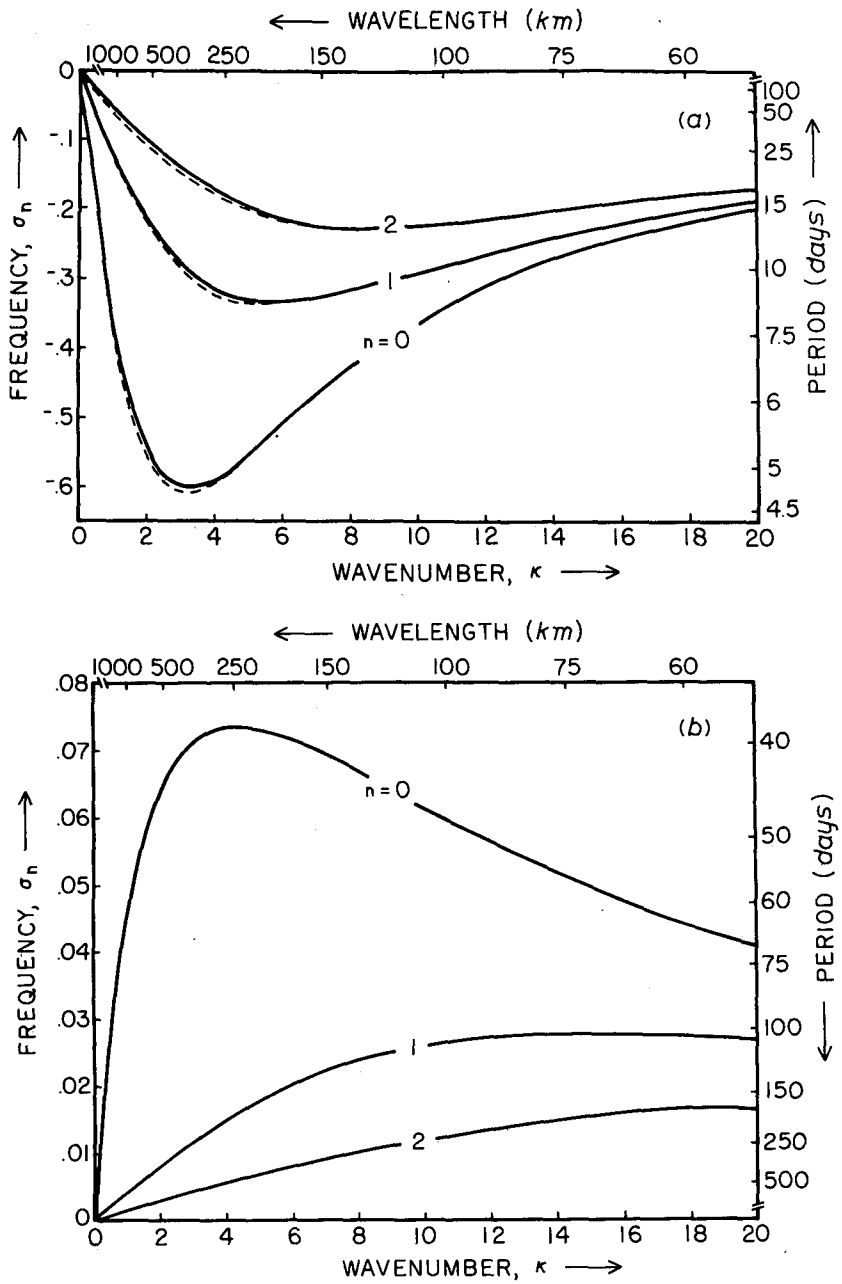

FIG. 4. The shelf wave (a) and trench wave (b) dispersion curves of the first three modes ($n = 0, 1, 2$) computed from Eqs. (5.6) and (5.13), respectively, for $a = 2.04$, $b = 0.49$ and $r = 0.29$ (Peru shelf/trench parameter values). The dashed curves in part (a) were computed from (5.7), the dispersion relation for shelf waves in the absence of a trench ($a = 2.04, b = 0, r = 0$). The values $L_1 = 171$ km and $|f| = 2.21$ rad day^{-1} (corresponding to 10.1°S latitude) were used to calculate wavelengths and periods respectively. Note that the vertical scale in (b) has been magnified tenfold over that in (a).

Examination of Table 1 reveals that the shelf/trench regions examined can be characterized by rather similar values of the geometrical parameters. We choose here, as representative cases, the Peru and Japan-Kuril values of a, b and r for the purposes of calculating the appropriate dispersion curves. These dispersion properties will be compared with phase propagation in sea level records from coastal stations bordering these trenches.

Fig. 4 shows the dispersion curves for shelf ($\sigma < 0$) and trench ($\sigma > 0$) waves off the coast of Peru. From Fig. 4 we note that the classical shelf

wave dispersion curves of Buchwald and Adams (1968) (the dashed lines) are hardly affected by the presence of a trench. The main effect of the trench is to decrease the frequency at intermediate wavenumbers by about 3–4%. The trench wave dispersion curves are similar in shape to those for the shelf waves. However, the zero group velocity for each trench wave mode occurs at a higher wavenumber. Further, the trench wave periods are about ten times longer than the shelf wave periods. As a consequence, their phase propagates very slowly (see Table 2 for values of the low-wavenumber phase speeds).

According to our coordinate system, y is directed southward along the Peru coast. Further, $f < 0$ in the Southern Hemisphere. It thus follows from (3.4) that the shelf waves, with $\omega_n > 0$, travel poleward (with the coast on the left), and that the trench waves, with $\omega_n < 0$, travel equatorward. The gravest mode shelf wave speed (143 km day^{-1}) compares favorably with the recent observations of Smith (1978) off the coast of Peru. He found that subinertial (0.05–0.25 cpd) fluctuations in current and sea level propagate coherently at 200 km day^{-1} in a poleward direction. If stratification were included in our model, the shelf wave speed would be increased (Mysak, 1967; Huthnance, 1978) and thus compare even more favorably with the observed speed. Smith suggested that these fluctuations may represent baroclinic Kelvin waves, especially in the region 10–15°S. However, in the latitude band 8–13°S, where our profile fits were made, it is suggested that these propagating signals may instead be interpreted as shelf waves.

Fig. 5 shows the shelf and trench wave eigenfunctions corresponding to the modes shown in Fig. 4. All the eigenfunctions are plotted for $\kappa = 1$, with the corresponding values of σ_n found in Fig. 4. As pointed out earlier, the shelf wave eigenfunctions are oscillatory only over the shelf region ($-1 < x' < 0$), whereas the trench wave eigenfunctions are oscillatory only over the trench. In each case, however, the nth mode eigenfunc-

TABLE 2. Phase speeds c_n ($=\omega_n/k$) of nondispersive shelf and trench waves for the Peru and Chile coasts. All speeds are given in units of km day^{-1}.

	Mode number n	Phase speed	
		Shelf waves	Trench waves
Peru	0	143	21
	1	43	1.7
	2	18	0.57
Chile	0	224	75
	1	52	5.6
	2	22	1.9

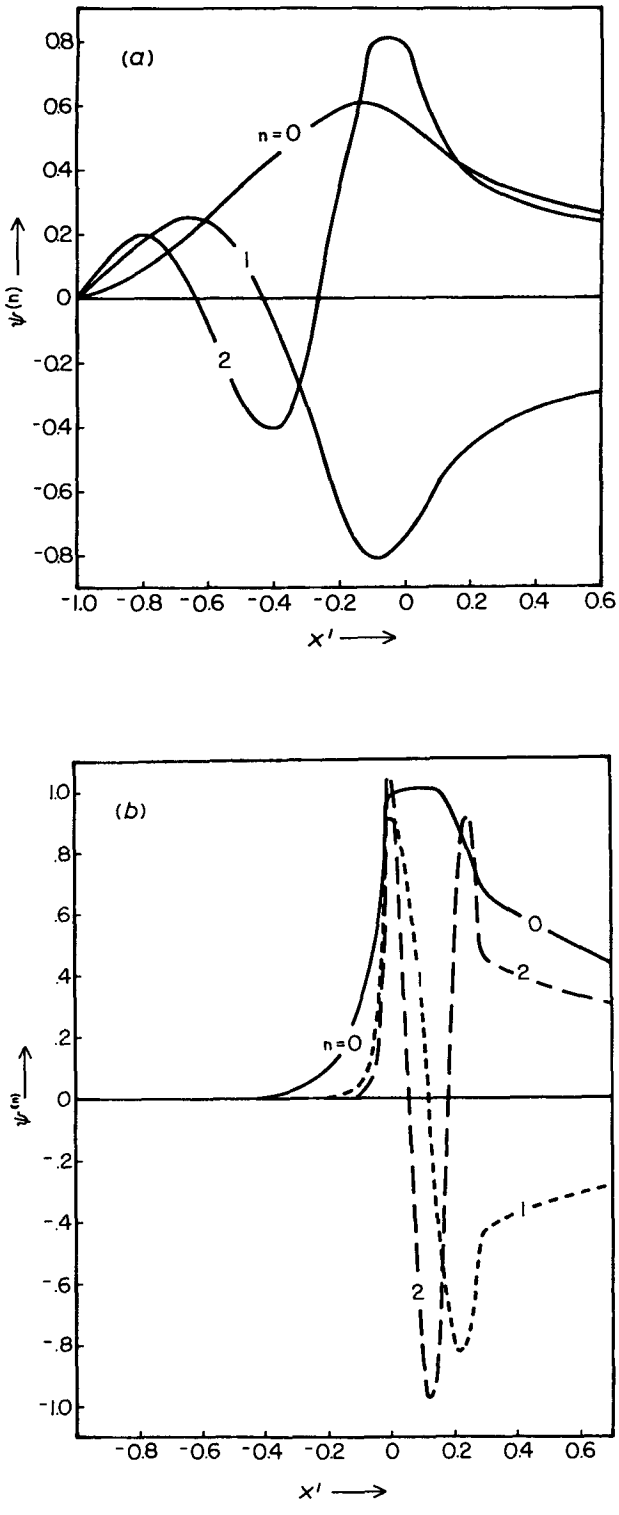

FIG. 5. The shelf wave (a) and trench wave (b) eigenfunctions $\psi^{(n)}$ of the first three modes computed from Eqs. (5.10) and (5.18), respectively, for $a = 2.04$, $b = 0.49$, $r = 0.29$ (Peru shelf/trench parameter values) and $\kappa = 1$. The eigenfunctions $\psi^{(0)}$, $\psi^{(1)}$, $\psi^{(2)}$ computed from (5.18) were normalized by multiplying with the factors 10^{-4}, 10^{-13}, 4×10^{-22}, respectively, before being plotted in (b).

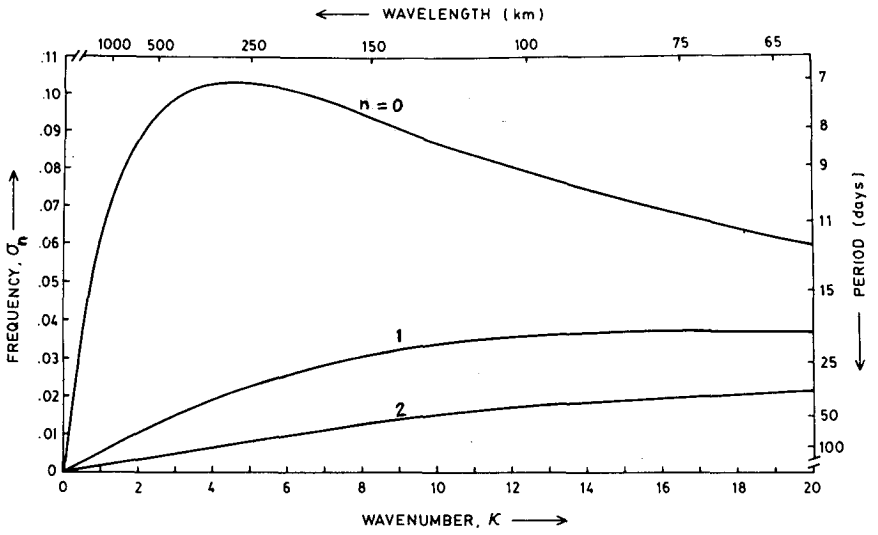

FIG. 6. The trench wave dispersion curves of the first three modes for the combined Japan-Kuril trench.

tion has n zero crossings. It is interesting to note that the trench waves are very strongly trapped over the trench region ($0 < x' < r$). Thus any nonlinear interactions that may occur between shelf and trench waves will have their largest energy exchanges over the trench region.

The dispersion curves for the combined Japan-Kuril trench are given in Fig. 6. The general character is much the same as the Peru trench with faster nondispersive phase speeds (Table 3) off Japan. Phase speeds are given for both the Japan and Kuril trenches separately as well as for the combined trench system.

6. Sea level records

Monthly sea level data for stations in Japan, the Kuril Islands and Kamchatka were studied to determine if phase propagation, consistent with trench wave dynamics, could be detected. Data starting August 1957 and running to December 1966 provided a continuous record of 653 monthly values for the eight stations from Petropavlosk (Fig. 2) in the north to Mera in the south. These data were adjusted for atmospheric pressure.

TABLE 3. Phase speeds c_n ($=\omega_n/k$) of nondispersive trench waves for the Japan, Kuril and combined Japan-Kuril trenches. All speeds are given in km day^{-1}.

Mode number n	Phase speed		
	Japan	Kuril	Japan-Kuril
0	82.5	224	152
1	5.78	13.8	9.3
2	1.83	4.0	2.96

Lag correlations were computed for all station pairs for lags up to 12 months. The maximum correlation, in this interval, was determined and the corresponding lag plotted against the separation distance between the appropriate sea level stations (Fig. 7). The shift of lag with distance suggests northward propagation consonant with trench wave behavior.

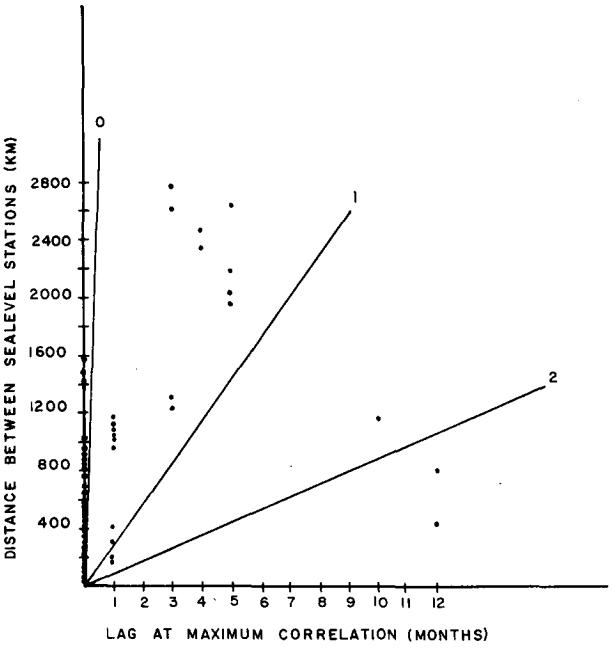

FIG. 7. Lag in months at the maximum correlation between sea level stations along the Japan-Kuril trench versus the separation distance (km) between stations. The lines corresponding to the nondispersive phase speeds of the first three trench wave modes are also shown.

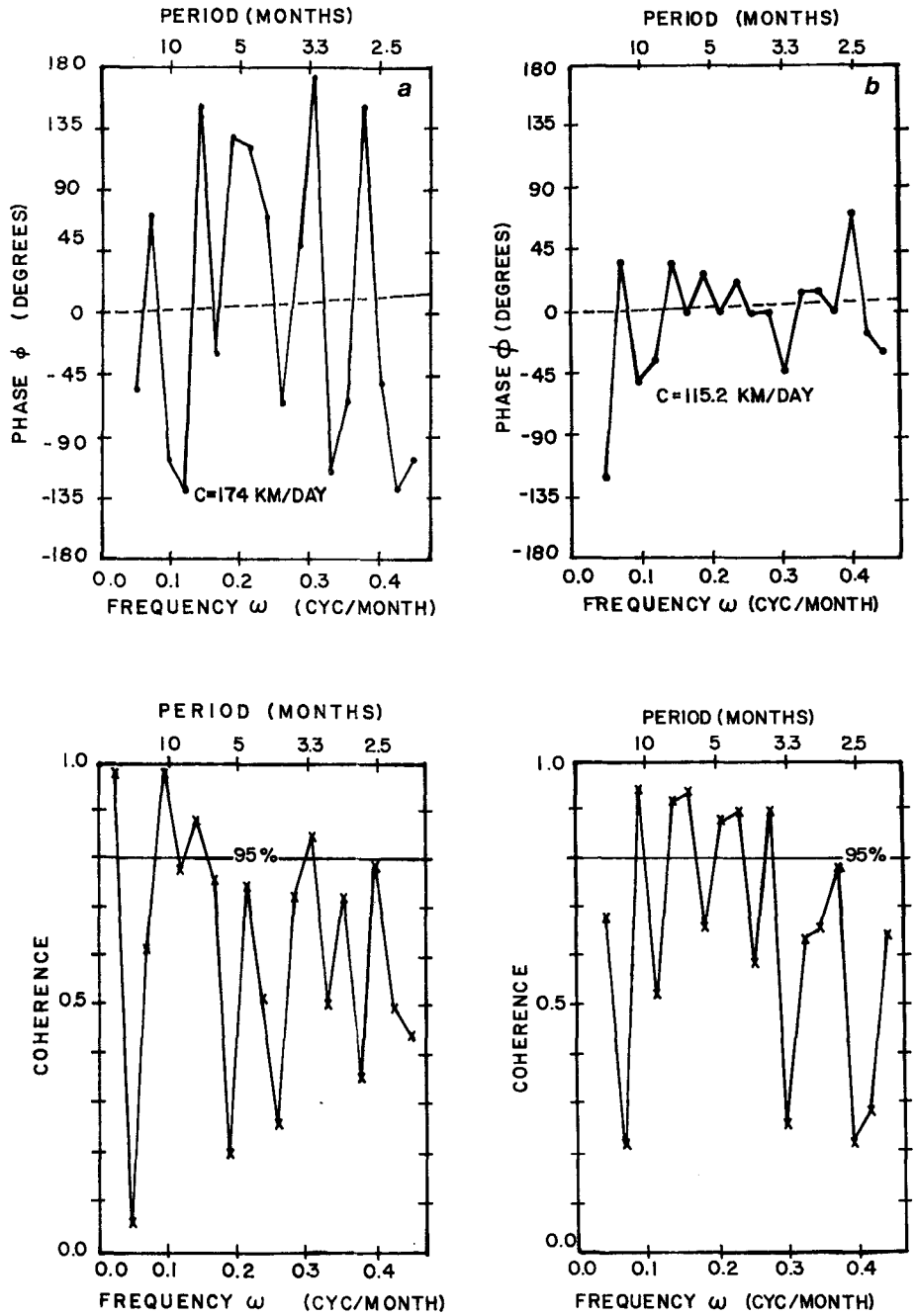

FIG. 8. Phase and coherence spectra of monthly sea level data between (a) Mera and Petropavlosk, separation = 2605 km, and (b) Onahama and Yuzno Kurilisk, separation = 892 km. Phase propagation is indicated by dashed lines in the phase spectra.

Plotting lines of the nondispersive phase speed for the first three modes (combined trench) indicates the possible presence of all three. First and second mode speeds are represented by only two or three points with the majority of points lying along the ordinate. These values, at zero lag, may be explained by the very fast phase speed of the fundamental mode (Table 3). Another group of points, at wide separation distances, suggests a combination of fundamental and first modes.

Assuming that trench waves propagate nondispersively, phase propagation should result in a straight line in the phase spectrum and high coherence in the coherence spectrum. Cross spectra were computed for all pairs of sea level stations shown in Fig. 1. A straight line weighted by the

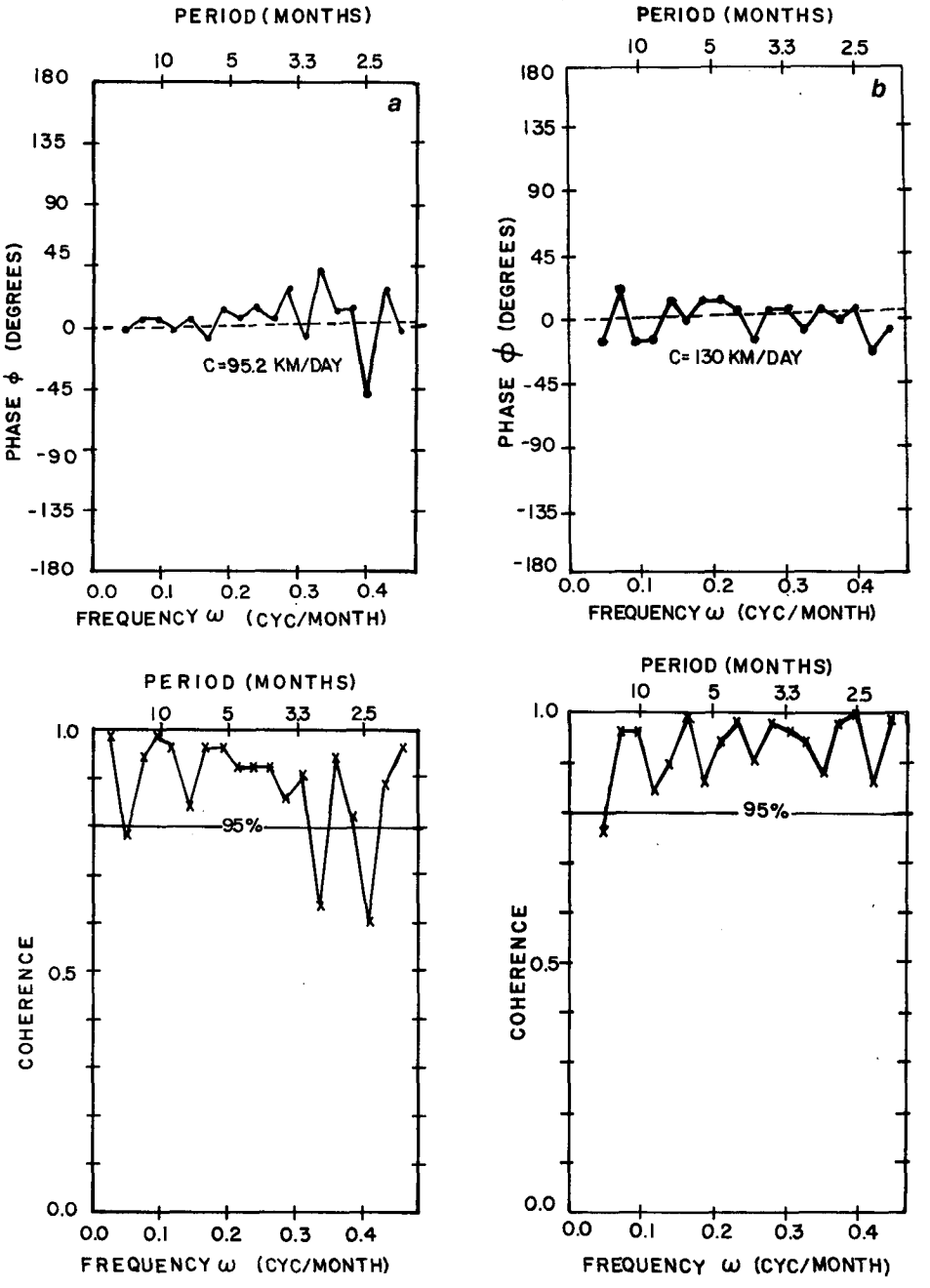

FIG. 9. As in Fig. 8 except for (a) Onahama and Hachinohe, separation = 400 km and (b) Kushiro and Hanasaki, separation = 102 km.

coherence, was fitted to each phase spectrum. About 75% of the station pairs exhibited northward propagation by positive slopes, consistent with trench wave theory. The speeds associated with these phase lines are close to that of the fundamental trench wave mode.

Selected examples of such phase spectra, along with the corresponding coherence spectra, are presented in Figs. 8 and 9. The 95% confidence level for coherence was determined as described in Julian (1975). Although the phase oscillates widely in Fig. 8a the linear fit, weighted by the coherence, indicates a phase speed of 174 km day^{-1} somewhat higher than 152 km day^{-1} given in Table 3 for the combined trench fundamental mode. A station pair with half the separation (Fig. 8b) yielded a phase speed of 115.2 km day^{-1}. Even closer station pairs in Figs. 9a and 9b gave speeds of 95.2 and 130 km day^{-1}, respectively. There appeared to be no clear correspondence between phase speed and station

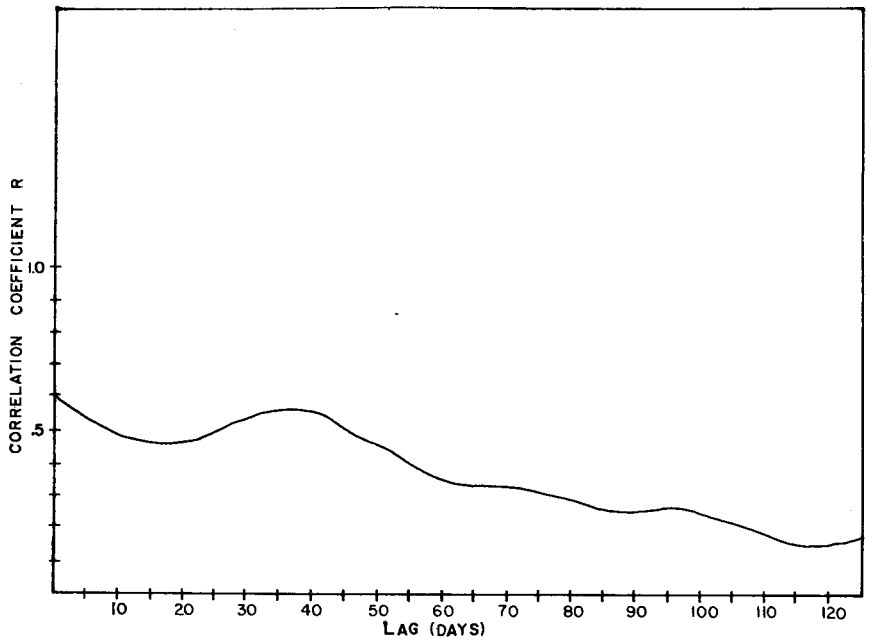

FIG. 10. Lag-correlation plot for daily sea level data between Talara and Matarani.

separation. Most of the values were slightly below that of the fundamental mode. Some phase spectra (~25%) exhibited negative slopes (southward propagation) with similar phase speeds. These negative slopes occurred mainly for closely spaced stations along the southern coast. It is possible that local topographic features could lead to sea level fluctuations that would mask the effects of the trench waves.

Such an effect was clearly noted in the analysis of daily sea level records from three stations in Peru (Fig. 2). Using data from the period between 1972 and 1974, 1884 daily values were used in a lag correlation analysis. These data were not corrected for atmospheric pressure as Smith (1978) had demonstrated that such correction did not significantly alter the correlation study of shelf waves. A plot of correlation versus lag for the northernmost (Talara) and southernmost (Matarani) stations (Fig. 10) is highest at zero lag, with a secondary maximum at 37 days. In an effort to sense any possible phase propagation similar plots were made for Callao-Talara and Callao-Matarani. No shift in the lag of the secondary maximum was evident, however.

The power spectra of these data revealed some interesting differences between these three stations. While Talara and Matarani both appeared to fall off with frequency, Callao had large, rounded peaks at periods of 4.5, 2.7 and 2.0 days. Similar peaks are present in the power spectrum of sea level at Callao, computed from data collected after 1974 (Smith, 1978).

This different spectral character at Callao may explain why the phase spectra for both pairs using Callao fluctuate widely and the coherence is uniformly low. In contrast the phase and coherence spectra (Fig. 11) for Matarani and Talara show high coherence for the periods around 37 days and a corresponding equatorward phase speed of 54 km day^{-1}, twice that of the fundamental mode (Table 2). The line of phase propagation was computed using, as before, the coherence spectrum as a weighting function. The fit was not continued for periods shorter than 20 days which is well out of the nondispersive regime. Although the velocity is larger than that predicted for Peru alone, it is in the right direction. It may be that since Matarani is situated at the Chile Trench the appropriate phase speed should be, as observed, between the 21 km day^{-1} given for Peru and the 75 km day^{-1} given for Chile (Table 2).

The presence of the Nazca Ridge, just south of Callao, may explain the anomalous behavior at this station. This ridge protrudes at right angles to the trench system and may disrupt the topographic waveguide sufficiently to alter the wave behavior at nearby Callao. Farther up the coast the wave reestablishes itself and is again detectable at Talara.

7. Conclusions

The main conclusions to be drawn from this study are as follows:

1) Most coastal trenches in the Pacific can be

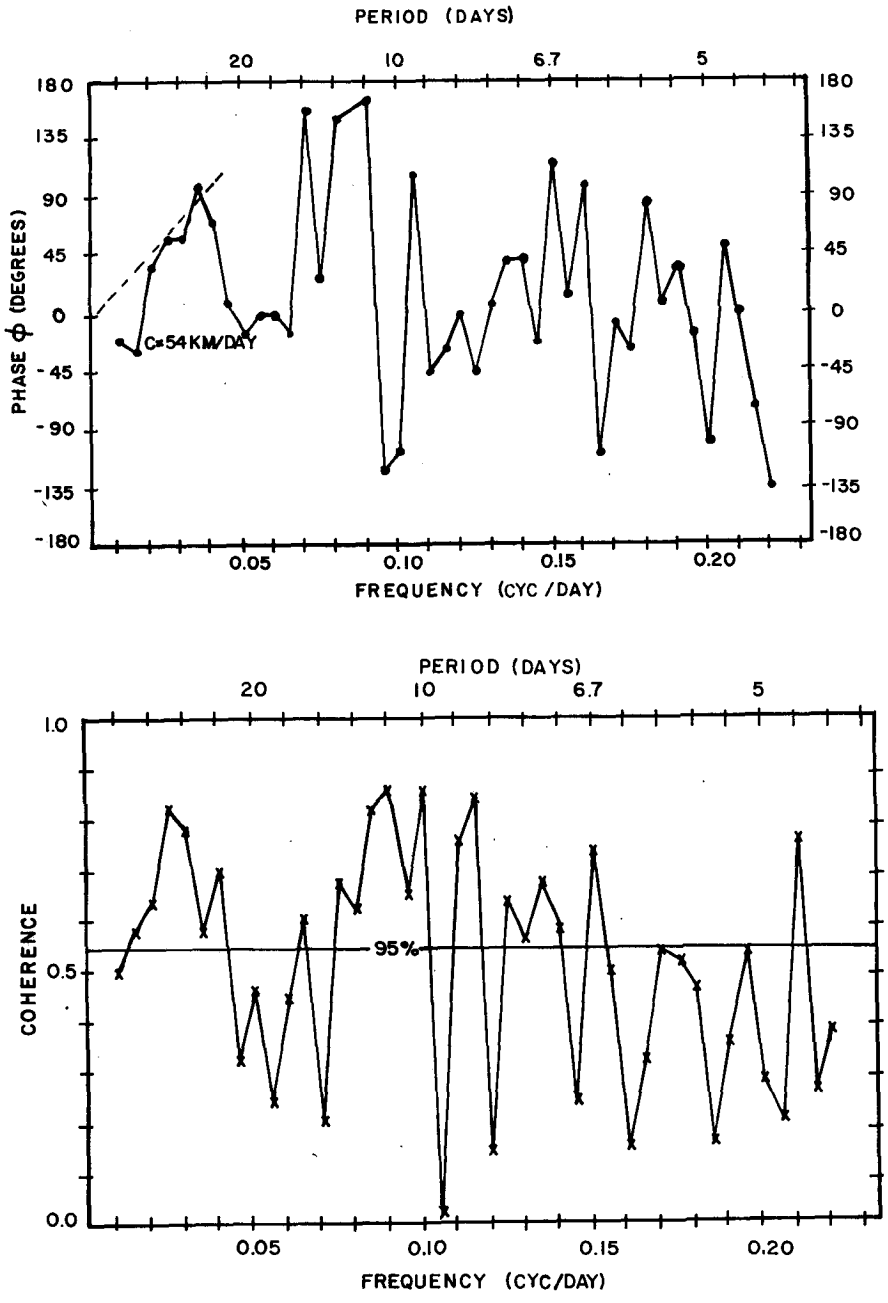

FIG. 11. Phase and coherence spectra of daily sea level data between Talara and Matarani. Phase propagation is indicated by a dashed line.

accurately fitted by a pair of exponential depth profiles with slopes of opposite sign.

2) Over such a shelf/trench profile there exists two types of second-class trapped waves: shelf waves and trench waves. The phase of the shelf waves propagates in the direction prescribed by the usual criterion for topographic waves, and the phase of the trench waves travels in the opposite direction. Trench waves have characteristic periods of 100 days, an order of magnitude longer than shelf wave periods.

3) The presence of an offshore trench slows down the conventional shelf waves of Buchwald and Adams (1968) by at most a few percent.

4) Monthly sea-level data along the Japan-Kuril trench and daily sea level data along the Peru trench exhibit phase propagation consistent with trench wave dynamics. Cross correlations and

cross-spectral analysis indicated phase propagation in the right direction at speeds representative of the fundamental mode.

Acknowledgments. This work was partly supported by the National Research Council of Canada. Thanks are due to David Cumming for carrying out the many computations and plotting the graphs.

The sea level data were kindly provided by Klaus Wyrtki. The data analysis was supported in part by the U.S. Office of Naval Research, Code 481. This support is gratefully acknowledged.

REFERENCES

Buchwald, V. T., and J. K. Adams, 1968: The propagation of continental shelf waves. *Proc. Roy. Soc. London*, **A305**, 235–250.

Hamon, B. V., 1962: The spectrum of mean sea level at Sydney, Coff's Harbour, and Lord Howe Island. *J. Geophys. Res.*, **67**, 5147–5155.

——, 1963: Correction to "The spectrum of mean sea level at Sydney, Coff's Harbour, and Lord Howe Island". *J. Geophys. Res.*, **68**, 4635.

Huthnance, J. M., 1975: On trapped waves over a continental shelf. *J. Fluid Mech.*, **67**, 689–704.

——, 1978: On coastal trapped waves: Analysis and calculation by inverse iteration. *J. Phys. Oceanogr.*, **8**, 74–92.

Julian, P. R., 1975: Comments on the determination of significance levels of the coherence statistic. *J. Atmos. Sci.*, **32**, 836–837.

LeBlond, P. H., and L. A. Mysak, 1977: Trapped coastal waves and their role in shelf dynamics. *The Sea*, Vol. 6, E. D. Goldberg *et al.*, Eds., Wiley-Interscience, 459–495.

——, and ——, 1978: *Waves in the Ocean*. Elsevier, 602 pp.

Louis, J. P., 1978: Low-frequency edge waves over a trench-ridge topography adjoining a straight coastline. *Geophys. Astrophys. Fluid Dyn.*, **9**, 229–239.

Mysak, L. A., 1967: On the theory of continental shelf waves. *J. Mar. Res.*, **25**, 205–227.

Smith, R. L., 1978: Poleward propagating perturbations in currents and sea level along the Peru Coast. *J. Geophys. Res.*, **83**, 6083–6092.